# Characteristic compressive properties of hybrid metal matrix syntactic foams

Kornél MÁJLINGER[a,c], Imre Norbert ORBULOV[a,b,d,*]

Department of Materials Science and Engineering, Faculty of Mechanical Engineering, Budapest University of Technology and Economics, Bertalan Lajos utca 7., Budapest, Hungary, 1111

[b]MTA–BME Research Group for Composite Science and Technology, Műegyetem rakpart 3., Budapest, Hungary, 1111

[c]vmkornel@eik.bme.hu

[d]orbulov@eik.bme.hu

*Corresponding author

Address: Department of Materials Science and Engineering, Faculty of Mechanical Engineering, Budapest University of Technology and Economics, Bertalan Lajos utca 7., Budapest, Hungary, 1111

Tel: +36 1 463 2386

Fax: +36 1 463 1366

E-mail: orbulov@eik.bme.hu, orbulov@gmail.com

**Abstract** Hybrid metal matrix syntactic foams (hybrid MMSFs) are particle reinforced composites in which the reinforcement is the combination of more than one grade of hollow spheres. The difference between the spheres can be in their chemical composition, dimension, physical properties etc. In this study AlSi12 matrix hybrid MMSFs with monomodal Globocer ($Al_2O_3$ and $SiO_2$ based ceramic) and Globomet (pure Fe) reinforcements were produced by pressure infiltration. The investigation parameters were the ratio of the hollow sphere grades and the aspect ratio of the specimens. Microstructural investigations showed almost perfect infiltration and favourable interface layer, while quasi-static compression tests showed that the composition of the reinforcement and the aspect ratio of the specimens have determinative effect on the characteristic properties (compressive and flow strength, fracture strain, stiffness and absorbed energy). This nature of the MMSFs ensures the possibility to tailor their properties in order to optimise them for a given application.

**Keywords:** Mechanical characterisation; Cellular materials; Metal matrix composites; Fracture; Syntactic foam

## 1. Introduction

Metal matrix syntactic foams (MMSFs) are special particle reinforced composites that consist of a metal matrix (usually some kind of Al or Mg alloy, to get maximal weight reduction) and a set of hollow, spherical particles. Most commonly the hollow spheres are built up from some sort of ceramic or metallic material and they are commercially available [1-5]. MMSFs have outstanding mechanical properties, like higher strength, stiffness and energy absorption capacity compared to other metallic foams, while their fracture strain is usually lower. Due to this, the MMSFs have promising

application possibilities as lightweight parts or as hulls of public and/or military vehicles [6, 7], as well as collision or vibration dampers.

In most cases MMSFs are made by stir casting or infiltration. Stir casting is cheaper and faster, but it can only produce lower reinforcement volume fractions due to hollow sphere breakage caused by mechanical stirring [8-16]. In the case of infiltration two basic methods can be separated: gravity-fed infiltration (only in the case of wetting matrix – reinforcement systems [17-20]) and pressure-assisted infiltration (for non-wetting systems). In the latter case a threshold pressure must be overcome in order to get acceptable workpieces. The threshold pressure can be calculated (estimated) [21-28] or measured [29-31]. Pressure infiltration is capable of producing MMSFs with maximal (~64 vol%) hollow sphere volume fraction and better matrix dispersion, but it requires more investment and more sophisticated equipment [29, 30, 32-38]. In practice, usually one kind of hollow sphere set with monomodal diameter distribution is applied as reinforcement. Only a few efforts have been published about MMSFs with bimodal hollow sphere diameter distribution [39]. Daoud [10] produced closed cell foams by gas releasing method and added hollow spheres into the ZnAl12 base metal. This hybrid foam showed ductile compressive deformation and exhibited higher mechanical strength than pure ZnAl12 foams. Xia et al. [40] produced and investigated Al99.5 based closed cell foams with different kinds and contents of ceramic microspheres in the cell walls by melt-foaming method. They showed that the microspheres have a significant effect on the strength, the deformation capabilities and the energy absorption of the foams. However – according to the best knowledge of the authors – no research results have been published about other hybrid MMSFs containing at least two different reinforcement grades. The difference between the reinforcements can be in the mean dimension,

chemical composition, physical properties etc. For example, in the case of MMSFs the material of the spheres can be different: metal and ceramic hollow spheres can be combined.

The most common loading mode of the foams is compression. Therefore the compressive properties of MMSFs have been widely studied and the quasi-static testing method has been standardised in DIN50134 [41]. Balch et al. [42, 43] examined the compressive properties and the load partitioning mechanisms in aluminium based syntactic foams (ASFs). According to their results optimised properties can be reached when the matrix and hollow spheres strengths are properly matched. Dou et al. [44] performed quasi-static and high strain rate compression tests on ASFs. The results showed distinct strain rate sensitivity. Goel et al. [45] investigated the dynamic compressive properties of ASFs. They showed that the compressive strength and energy absorption attained an optimum at a given strain rate. Kiser et al. [46] investigated ceramic hollow sphere reinforced ASFs under compressive loads. Uniaxial compressive failure has been initiated at small strains through the collapse of the material within a localized deformation band. Under constrained conditions, localization was suppressed and the flow stress increased monotonically. Different matrix (Mg and Zn alloys) syntactic foams were studied by Rohatgi et al., Daoud [8, 9, 47, 48] and Huang et al. [49, 50]. The hollow spheres decreased the density and the foams became stiffer and stronger, than the conventional ones. Castro and Nutt [20, 51] investigated the synthesis of steel matrix syntactic foams with $Al_2O_3$ hollow spheres. The MMSFs exhibited higher strength and energy absorption capacity than the steel foams reported previously. The compression and low-velocity impact behaviour of ASFs were also studied by the same research group [52]. Luong et al. [53-55] investigated the strain rate sensitivity

of Al and Mg based syntactic foams. The MMSFs showed higher strength and higher energy absorption capability at higher strain rates. Mondal et al. [13, 14] reported stir-casted ASFs behaved like high strength Al foams under compressive deformation, both at room and elevated temperature. The plateau stress decreased with hollow sphere volume fraction, following a power law relationship. Neville and Rabiei [56] produced MMSFs by a powder metallurgy technique. The materials displayed superior strength to density and absorbed energy to density ratios [17, 57, 58]. Palmer et al. [32] studied the compressive properties of ASFs with different size ceramic hollow spheres and various Al alloy matrices. The alloy-sphere-temperature combinations gave potential for tailoring these materials for different applications. Peroni et al. [59, 60] investigated the mechanical behaviour of MMSFs made of hollow glass spheres mixed in iron matrix. The produced materials offered greatly increased quasi-static compressive strength, though at higher density. Rohatgi et al. [35] performed compressive tests on ASFs containing different volume fractions of hollow spheres. The strength and stiffness increased with the increasing density. The microstructure and quasi-static compressive mechanical properties of ASFs with $Al_2O_3$ hollow spheres were investigated and estimated by [61-63] in different conditions. The peak and plateau strength as well as the toughness of the foams increased with increasing wall thickness to diameter ratio. ASFs with additional Al particles were produced by Tao et al. [64, 65] via pressure infiltration. The ductility, the strength and the specific energy absorption capacity increased significantly. Different failure modes (progressive collapse and/or Griffith rupture) were observed in confined and unconfined compression as well. Wu et al. [66] performed quasi-static compression tests on ASFs: the annealed ASFs could deform plastically at a relatively high stress. A method was also established to show the relation between

the relative wall thickness of the hollow spheres and the compressive strength. Zhang and Zhao [36] investigated the mechanical response of ASFs with low-cost porous ceramic hollow spheres under static and dynamic conditions. The plateau strength and the absorbed energy were largely determined by the volume fraction of Al and to a lesser extent by the properties of the hollow spheres. Zou et al. [67] studied the dynamic mechanical behaviour of ASFs produced by pressure infiltration. During the deformation process, the ASFs exhibited good energy absorption capability. Orbulov et al. [68-71] investigated the characteristic properties (compressive strength, fracture strain, structural stiffness and absorbed energy) of ASFs. In these studies, versatile combinations of matrix materials, hollow sphere grades and testing conditions (aspect ratio, test temperature, heat treatment etc.) were applied. The results showed outstanding specific mechanical properties under any circumstances.

The elastic properties of the MMSFs can be estimated via mathematical and mechanical considerations. Bardella et al. [72-75], Mondal et al. [76, 77] and Marur [78-81] investigated the analytical and numerical modelling of MMSFs. Their main aim was to predict the elastic properties and to model the load transfer of MMSFs in different circumstances, including interfacial quality. The interface layer was investigated experimentally by Orbulov et al. [82-84] on microstructural scale. Chemical exchange reactions were observed and confirmed that can alter the quality of the interface layer, and through this, have a serious effect on the mechanical properties. Moreover Orbulov et al [85, 86] gave the analytical description of the behaviour of ASFs that can be applied to model MMSF parts numerically.

As it is presented above, the mechanical properties of MMSFs have been more or less widely measured, but data about hybrid MMSFs is lacking. Therefore the aim of

this paper is to give detailed introduction to the mechanical and microstructural properties of hybrid MMSFs.

## 2. Materials and experimental methods

### 2.1. Investigated materials and production method

Near eutectic AlSi12 alloy (Al4047) was used as matrix material due to its low melting point (~575°C) and low viscosity. The measured chemical composition of the matrix was: 12.830 wt% Si, 0.127 wt% Fe, 0.002 wt% Cu, 0.005 wt% Mn, 0.010 wt% Mg, 0.007 wt% Zn and the remaining was Al. This composition is in the range of the standardised nominal values [87]. The total amount of reinforcement was maintained at high level (~64 vol%) that corresponds to the randomly close packed structure (RCPS [88, 89]) in all cases. The reinforcement consisted of two different grades of hollow spheres (one ceramic and one metal) manufactured by Hollomet GmbH [1]. The ceramic hollow spheres (Globocer, GC) had the average diameter and wall thickness of Ø1425±42.2 μm and t=60±1.7 μm respectively, while their density was ρ=0.816 $gcm^{-3}$. The chemical composition of the hollow sphere's wall material was 33 wt% $Al_2O_3$, 48 wt% $SiO_2$ and 19 wt% $3Al_2O_3 \cdot 2SiO_2$. The metallic hollow spheres (Globomet, GM) had the similar average diameter (Ø1413±21.5 μm) but smaller wall thickness (t=23±0.6 μm), while the density was ρ= 0.704 $gcm^{-3}$. The fracture force of GC and GM grade hollow spheres between polished plates was 22.1±1.18 N and 5.1±0.18 N (50-50 measurements) respectively, so the GC grade hollow spheres proved to be significantly stronger. The GC and GM grade hollow spheres showed brittle fracture and plastic failure, respectively. The ratio of the hollow spheres varied from 100% GC and 0% GM to 0% GC and 100% GM, in 20% steps.

The hybrid ASFs were produced by inert gas (Ar) assisted pressure infiltration (Fig. 1). First, the hollow sphere grades were hand-mixed carefully to reach uniform ratio

of them throughout. This could be ensured by hand-mixing, because the density difference between the grades is quite small. The mixed hollow spheres were poured into a graphite coated carbon steel mould (height: 360 mm, cross section: 40×60 mm, wall thickness: 3 mm) to the half and they were compacted by gentle tapping to get RCPS (64 vol%, [88, 89]). Subsequently, a layer of alumina separator was placed on the hollow spheres and a block of matrix material was put on the mat. The mould was placed into the infiltration chamber; the furnace was closed and evacuated by a vacuum pump (rough vacuum). The heating was ensured by three heating zones and the temperatures of the matrix block and the hollow spheres were continuously monitored by two thermocouples. After melting and overheating to the infiltration temperature (625°C) the molten metal sealed the mould above the separator layer. The vacuum pump was switched off and Ar gas was let into the chamber with a previously set 400 kPa pressure. The pressure difference (400 kPa in the chamber and vacuum under the liquid) forced the molten metal to infiltrate into the space between the hollow spheres. The system was cooled down to 550°C in Ar gas. After solidification the mould was removed from the chamber and water cooled to room temperature. Then the ASF block (~40×60×180 mm) could be removed from the mould. For further details about the production process please, refer to [29, 68]. The blocks were designated after their constituents: e. g. 20GC+80GM stands for an ASF block with AlSi12 matrix and with ~64 vol% of hollow spheres that is mixed from 20 vol% GC and 80 vol% GM grade hollow spheres respectively. The measured densities ($\rho_m$) of the blocks, determined by Archimedes' method, are listed in Table 1.

**2.2. Experimental**

An Olympus PMG3 type light microscope was used to investigate the microstructure of MMSFs and the quality of the infiltration. Scanning electron microscopy (SEM)

investigations and energy dispersive spectrometry (EDS) were performed on polished surfaces along distinguished lines by a Phillips XL-30 type electron microscope equipped with an EDAX Genesis EDS analyser. The measurement started from the matrix materials and crossed the wall of the hollow sphere perpendicularly. Thirty points were measured along each line. Each point was excited for 15 s with 35 μs detector amplification time.

The compressive properties were investigated in quasi-static conditions on cylindrical specimens. Besides the hybrid reinforcement structure the aspect ratio (height to diameter ratio, H/D) of the specimens were varied: the diameter (D) of the specimens was 14 mm and the height (H) was 14, 21 or 28 mm (H/D 1, 1.5 and 2 respectively). The compression tests were performed on a MTS 810 type universal testing machine in a four column equipment at room temperature. The acting surface of the dies was ground and polished. The specimens and the dies were lubricated with Locktite anti-seize material. The test speed was 0.01 $s^{-1}$. Five specimens were compressed from each specimen group up to 25% engineering strain to get representative results and to verify repeatability. Overall 90 specimens were compressed (6 material types (Table 1) × 3 aspect ratios × 5 specimens). The results were evaluated according to the standard concerning the compression tests of cellular materials [41] and the characteristic properties (compressive and flow strength, fracture strain, structural stiffness and absorbed energies) were determined.

## 3. Results and Discussion

### 3.1. Microstructure

The microstructure of the ASFs has to be analysed from two points of view. First, the production method (in this case pressure infiltration) should be qualified in terms of porosity between the hollow spheres. Secondly, the interface layer between the

reinforcement and the matrix material should be investigated, because this layer is responsible for the proper load transfer between the constituents and therefore has determinative effect on the mechanical properties. The quality of infiltration can be investigated by light microscopy. Fig. 2 shows typical areas about 20GC+80GM ASFs at low magnifications. The ceramic (light circles) and the metal (dark circles) hollow spheres can be easily separated in the grey aluminium matrix. The micrographs show almost perfect infiltration, even the smallest cavities between the hollow spheres were infiltrated almost completely by the AlSi12 matrix. The uninfiltrated void content between the hollow spheres was investigated by optical microscopy in different (randomly chosen) sections. According to the microscopic investigations the uninfiltrated void content is well below 3% (compared to the volume of the matrix). Some broken and therefore filled hollow spheres can be observed in Fig. 2, which can occur if a hollow sphere breaks during infiltration or if it is already broken before infiltration. In most cases the broken spheres are GM grade, because the molten AlSi12 – as a chemically aggressive medium – can dissolve pure Fe from the wall and it can lead to the breakage and infiltration of these hollow spheres (Eq. 1-3).

$$Al_{(liq)} + Fe_{(sol)} \rightarrow Fe - Al_{(sol)} \quad \text{(Eq. 1)}$$

$$3Al_{(liq)} + Fe_{(sol)} \rightarrow Al_3Fe_{(sol)} \quad \text{(Eq. 2)}$$

$$Fe_{(sol)} + Si_{(liq)} \rightarrow FeSi_{(sol)} \quad \text{(Eq. 3)}$$

In the case of ceramic hollow spheres the Al content of the matrix can dissolve Si from the wall of the spheres according to Eq. 4.

$$4Al_{(liq)} + 3SiO_{2(sol)} \rightarrow 2Al_2O_{3(sol)} + 3Si_{(sol)} \quad \text{(Eq. 4)}$$

This diffusion reaction is induced by the Si concentration mismatch between the material of the hollow spheres and the matrix. However, this exchange reaction is suppressed by the high Si amount in the matrix [82-84]. The investigation of the above mentioned and possible chemical reactions directly leads to the detailed analysis of the interface layer. The presence and thickness of the interface layer between the constituents can be investigated by line EDS analysis. A typical site of 60GC+40GM+ ASF is shown in Fig. 3. The SEM micrograph of a GM (left) and GC (right) hollow spheres near each other and the path of the line EDS analysis (arrow) are shown in Fig. 3a, while the chemical composition along the investigated line is plotted in Fig. 3b. The SEM micrograph shows unharmed hollow spheres and confirms the almost perfect infiltration: the less than 100 μm gap between the GM and GC grade hollow sphere is completely infiltrated. The chemical composition along the path of the analysis changes according to the composition of the wall and the matrix materials. The first few microns were measured in the GM grade hollow sphere and shows mainly Fe and some O due to the slight oxidation of the surface. Between the spheres the Al content is dominant, but Si peaks can be also observed due to the near-eutectic composition of the matrix material. In the GC grade hollow spheres the observed Al-Si-O ratio corresponds to the composition of the ceramic wall material. Sudden changes can be observed in the chemical composition in the interface layers between the GM and GC hollow spheres and the matrix material. These short transient zones indicate thin interface layers. The thickness of the layers can be estimated from the slope changes of the differentiated Fe and O curves and it is 5 μm and 7 μm in the case of GM and GC hollow spheres respectively.

In summary, the microstructural investigations verify the proper quality of the pressure infiltrated ASFs and promises convenient mechanical properties.

### 3.2. Compressive properties

Typical compressive stress-strain curves of the series of the ASFs with H/D=1 are shown in Fig. 4a; the amount of GC hollow sphere content improved the mechanical properties significantly. According to the standard [41] the compressive properties of the MMSFs can be sorted into strength, deformation and absorbed energy groups. The strength of MMSFs can be characterised by the first stress peak (compressive strength, $\sigma_c$) and by the strength at a given plastic deformation (similar to yield strength, $\sigma_y$). Another important stress property is the plateau strength ($\sigma_p$) that can be defined as the average stress between 5% and 25% deformation. The most important deformation parameter is the fracture strain ($\varepsilon_c$) that is the strain at $\sigma_c$. In the elastic zone the relation between the stress and strain can be described by structural stiffness (S), which is the slope of the initial part of the stress – strain curve (dashed line in Fig. 4b). In regards to the energy absorption of the MMSFs in this study, the fracture energy, $W_c$, is the energy absorbed up to the fracture strain, $\varepsilon_c$ (the cross-hatched area in Fig. 4b), and the total absorbed energy, W, is the total area under the measured stress-strain curve (hatched + cross-hatched area in Fig. 4b). The fracture energy and the total absorbed energy may be determined by the numerical integration of the stress-strain curves up to the fracture strain, or up to 25% strain respectively. The above specified characteristic properties are presented in Fig. 4b on the example of 40GC+60GM reinforced ASF having H/D=1.

Fig. 5a shows the compressive strength of the produced hybrid ASFs in the function of aspect ratio and the ratio of the hollow sphere grades. (In the case of pure GM reinforcement, significant compressive strength cannot be determined, therefore the yield strength is plotted (white bars) for comparison). There are some trends in the strength values: the specimens with lower H/D ratio are stronger and the

compressive strength also increases with the amount of GC reinforcement. The gradient of the latter increment is constant and moderate in the case of hybrid ASFs: as the proportion of the weaker, plastically deformable GM fraction decreases, the compressive strength increases. In the case of pure GC reinforcement a higher increment can be observed: the stronger GC hollow spheres and the lack of plastically deformable GM hollow spheres ensure higher strength levels. Exactly the same behaviour can be observed in the case of yield strength, as it is presented in Fig. 5b. The differences in the plateau stresses are significantly smaller (Fig. 5c), but the scatters are larger due to the unique build-up and deformation of each sample. However the above mentioned effects can be observed in the average values again. In Fig. 4a the comparison of the curves confirms this trend. The ASFs with pure GM grade reinforcement behave like conventional metallic foams. They have no significant compressive strength, but have a long, slowly increasing plateau region and completely plastic deformation. As the proportion of the GC hollow spheres increases the significant compressive strength become more and more emphasised and the failure mechanism changes to brittle mode with a single, sharp fracture band. These failure modes can be also observed in the microstructure as it is presented in Section 3.3 (Fig. 9). For better comparison the plotted numerical results are listed in Table 2.

The trends of fracture strain confirm the described effect of hollow sphere grade ratio (Fig. 6a, Table 3). As the amount of the GC hollow spheres increases, the fracture strain decreases and the failure mode becomes brittle. The aspect ratio also decreases the fracture strain: as the shearing effect becomes more intensive due to the larger aspect ratio, the fracture occurres earlier [69]. This effect is more dominant in the case of higher GC content, because the ceramic materials are more sensitive

to shearing forces [68, 69]. The structural stiffness changes inversely (Fig. 6b, Table 3). The highest stiffness was measured in the case of H/D=2 at the highest GC content. The aspect ratio has an almost linear effect on the structural stiffness, but the ratio of the hollow sphere grades influences it exponentially with the increment of the GC hollow sphere fraction.

The absorbed mechanical energies are important in the case of safety and crashworthiness applications. The mechanical energy absorbed up to the fracture strain is called fracture energy. The fracture energy (Fig. 7a, Table 3) is maximal in the case of pure GC reinforcement: the strong ceramic hollow spheres ensure high compressive strength and high plateau stress level; therefore the absorbed energy (the area under the stress-strain curve) is high. As the weaker GM grade hollow spheres were added to the system the compressive strength and the fracture energy decreased. In the case of higher GM hollow sphere fraction (more than 40%) the fracture energy increases again: the decrement of the compressive strength is balanced by the higher deformation capability, i. e. the higher fracture strain of the ASFs. The higher fracture strain indicates higher integration limits during the numerical integration that is aiming the determination of the fracture energy. Due to this, fracture energy becomes higher despite lower compressive strength. The same behaviour can be observed in the case of the overall absorbed energy (up to 25%, Fig. 7b, Table 3). However the expected high energy absorption capacity cannot be observed in the case of pure GM hollow sphere reinforcement, due to its very low compressive and plateau strength.

As it is presented above (Fig. 4-7.) the mechanical properties can be altered within relatively wide ranges and it is possible to optimise the properties for a given or desired application. For future use - and also in the cases of not yet investigated Al

alloy matrices - it would be useful if the properties of hybrid ASFs could be predicted from the properties of pure GC and GM grade reinforced ASFs in order to save time and measurement efforts. The most obvious possibility for this aim is the rule of mixtures (Eq. 5).

$$P_{hybrid} = CP_{GC} + (1-C)P_{GM} \quad \text{(Eq. 5)}$$

Where $P_{hybrid}$ is the expected property of the hybrid ASF, C is the fraction of GC grade hollow spheres within the reinforcement, $P_{GC}$ and $P_{GM}$ is the property of pure GC and pure GM reinforced ASFs respectively. Eq. 5 is a linear relationship and it is presented in Fig. 8a and Fig. 8b in the case of yield and plateau strength and in the case of structural stiffness and fracture strain respectively. The lines represent the rule of mixture and the hashed areas correspond to the average scatter of the investigated property. Generally, Eq. 5 gives an acceptable prediction, but one important criterion exists: the total volume fraction of the reinforcement must be the same in the hybrid ASF and in the pure GC or GM reinforced ASF too.

Based on the above mentioned descriptions it is worth mentioning that by the application of different composite layers with different GC and GM ratio, gradient materials can be easily built according to the requirements of given applications. By proper mixing, build-up and/or by planned distribution (either one-by-one placement or altering ratio) of the different grade spheres, gradient behaviour in different direction(s) can be ensured for given parts. This property of hybrid ASFs allows application as energy absorbers, hulls, collision dampers or vibration dampers. The altering ratio of the reinforcing grades can also ensure unique failure modes built-up from the basic failure mechanisms described in the next section.

### 3.3. Failure modes

Ceramic hollow sphere reinforced MMSFs have three typical failure modes (A, B and C) depending on the reinforcement grade, size and on the aspect ratio, as it is introduced in [65, 69]. In mode A, two compression cones were formed at the top and at the bottom of the specimens. The failure started between the cones: first a few hollow spheres were broken, then the compressed zone expanded to a lens-like volume where the material was compressed and compacted; the specimen may also show some barrelling. The subsequent failure of the hollow spheres ensured high plateau strength and large mechanical energy absorption. This failure mode is similar to the fracture mode A and B as described by Tao and Zhao in [30] and normally it is frequent in the case of H/D=1 for all size of ceramic hollow spheres. In the case of mode B failure, one determined shear plane appeared in the specimen. The direction of the first rupture closed ~30° angle with the loading direction, as it was also observed in [65]. The rupture damaged one row of hollow spheres and divided the specimen into two halves. Subsequently, the shear band thickened and large part of the material remained unharmed. This confirmed the good damage tolerance and damage localising abilities. This failure mode occurred frequently in the case of higher aspect ratios, typically H/D=1.5 for GC grade reinforcement – as in our case as well. In the case of mode C failure, a cone like volume near to either end of the specimen started to deform and densified intensively. Due to this, additional radial forces began to act along the surface of the cones that split the specimens typically into three or four parts. This failure mode occurred only in the case of the largest aspect ratio (H/D=2) and in the case of small (Ø<500 μm) ceramic hollow sphere reinforcement, as it was detailed in [69].

The failure modes of MMSFs containing steel hollow spheres were investigated by Rabiei and Vendra: plastic deformation of the MMSFs was reported that corresponds to mode A failure [17, 58].

In the case of hybrid ASFs the combinations of the above mentioned failure modes were observed according to the ratio of the hollow grade spheres. As the fraction of GC grade hollow spheres increased the failure mechanism turned from brittle shearing (mode B, Fig. 9a) through mixed mode (Fig. 9b) to diffuse plastic collapse (mode A, Fig. 9c), as presented for 80GC+20GM, 60GC+40GM and 20GC+80GM ASFs respectively. All failure modes ensured higher mechanical energy capability than conventional metal foams.

## 4. Conclusions

From the above detailed investigations, the following conclusions can be drawn:

- Pressure infiltration is a convenient method to produce hybrid ASFs with high hollow sphere content and low uninfiltrated porosity.
- The SEM and line EDS analysis highlighted (i) solution of Fe from GM grade spheres into the AlSi12 matrix, that can cause damage to the wall and leads to infiltrated hollow spheres and (ii) an exchange reaction between the AlSi12 matrix and the GC grade spheres, that was suppressed by the high Si content of the AlSi12 matrix. The interface layers proved to be thin; the average layer thickness was less than 10 μm.
- The compressive and yield strength as well as the structural stiffness increased, while the fracture strain decreased as the GC grade hollow sphere fraction increased, respectively. By this nature, the basic mechanical properties of ASFs can be tailored properly for a given application.

- The absorbed mechanical energies were also influenced by the fraction of GM and GC grade hollow spheres and had a local minimum in the case of 60GC+40GM reinforcement. In the case of higher GC content the compressive and the plateau strengths were higher and therefore the absorbed energies became higher. In the case of lower GC content the strengths became lower, but the ductility of GM grade hollow spheres could balance and overcome this effect.
- The failure mode of the ASFs has changed between brittle shearing and plastic collapse according to the actual fraction of the hollow sphere grades.

**Acknowledgements**
This research was supported by the European Union and the State of Hungary, co-financed by the European Social Fund in the framework of TÁMOP 4.2.4. A/2-11-1-2012-0001 'National Excellence Program'.

**References**
[1] Hollomet GmbH (http://www.hollomet.com/home.html) (last accessed: 23th January 2014)
[2] Envirospheres Ltd. (http://www.envirospheres.com) (last accessed: 23th January 2014)
[3] Sphere Services Inc. (http://www.sphereservices.com/) (last accessed: 23th January 2014)
[4] 3M Company (http://solutions.3m.com/wps/portal/3M/en_US/3M-Defense-US/Defense/Products/~?N=5444948&rt=c3) (last accessed: 23th January 2014)
[5] Deep Springs Technology (http://teamdst.com/pdf/HollowShells_MTG119-A%20Web.pdf) (last accessed: 23th January 2014)
[6] R. Erikson, Mech. Eng. 121 (1999) 58-61.
[7] R. Erikson, Proceedings of 5th Aerospace Materials, Processes and Environmental Technology Conference. Huntsville, Alabama, USA, 2002, pp. 1-10.
[8] A. Daoud, M.T. Abou El-khair, M. Abdel-Aziz, P. Rohatgi, Compos. Sci. Technol. 67 (2007) 1842-1853.
[9] A. Daoud, Mater. Sci. Eng. A 488 (2008) 281-295.
[10] A. Daoud, Mater. Sci. Eng. A 525 (2009) 7-17.
[11] D.P. Mondal, S. Das, N. Jha, Mater. Des. 30 (2009) 2563-2568.
[12] N. Jha, A. Badkul, D.P. Mondal, S. Das, M. Singh, Tribol. Int. 44 (2011) 220-231.
[13] D.P. Mondal, N. Jha, A. Badkul, S. Das, R. Khedle, Mater. Sci. Eng. A 534 (2012) 521-529.
[14] D. P. Mondal, S. Das, N. Ramakrishnan, K. Uday Bhasker, Compos. Part A 40 (2009) 279-288.
[15] M. Ramachandra, K. Radhakrishna, Wear 262 (2007) 1450-1462.
[16] M. Ramachandra, K. Radhakrishna, J. Mater. Sci. 40 (2005) 5989-5997.
[17] L.J. Vendra, A. Rabiei, Mater. Sci. Eng. A 465 (2007) 59-67.
[18] A. Rabiei, A.T. O'Neill, Mater. Sci. Eng. A 404 (2005) 159-164.

[19] K.P. Trumble, Acta Mater. 46 (1998) 2363-2367.
[20] G. Castro, S.R. Nutt, Mater. Sci. Eng. A 553 (2012) 89-95.
[21] E.W. Washburn, Phys. Rev. 17 (1921) 273-283.
[22] K.A. Semlak, F.N. Rhines, Trans. Metall. Soc. AIME 16 (1958) 325-331.
[23] R. Asthana, P.K. Rohatgi, S.N. Tewari, Process. Adv. Mater. 2 (1992) 1-17.
[24] D. Muscat, R.A.L. Drew, Metall. Mater. Trans. A 25 (1994) 2357-2370.
[25] C. Garcia-Cordovilla, E. Louis, J. Narciso, Acta Mater. 47 (1999) 4461-4479.
[26] V.M. Kevorkijan, Compos. Sci. Technol. 59 (1999) 683-686.
[27] N. Eustathopoulos, B. Drevet, M.L. Muolo, Mater. Sci. Eng. A 300 (2001) 34-40.
[28] G. Kaptay, Proceedings of TMS 2001 fall meeting. Indianapolis, Indiana, USA, 2001, pp. 71-99.
[29] I.N. Orbulov, J. Dobránszky, Period. Polytech. Mech. Eng. 52 (2008) 35-42.
[30] I.N. Orbulov, Period. Polytech. Mech. Eng. 55 (2011) 21-27.
[31] I.N. Orbulov, Mater. Sci. Eng. A 583 (2013) 11-19.
[32] R.A. Palmer, K. Gao, T.M. Doan, L. Green, G. Cavallaro, Mater. Sci. Eng. A 464 (2007) 85-92.
[33] P.K. Rohatgi, R.Q. Guo, H. Iksan, E.J. Borchelt, R. Asthana, Mater. Sci. Eng. A 244 (1998) 22-30.
[34] P.K Rohatgi, N. Gupta, S. Alaraj, J. Compos. Mater. 40 (2006) 1163-1174.
[35] P.K. Rohatgi, J.K. Kim, N. Gupta, S. Alaraj, A. Daoud, Compos. Part A 37 (2006) 430-437.
[36] L.P. Zhang, Y.Y. Zhao, J. Compos. Mater. 41 (2007) 2105-2117.
[37] I.N. Orbulov, Á. Németh, J. Dobránszky, Mater. Sci. Forum 589 (2008) 137-142.
[38] I.N. Orbulov, J. Ginsztler, P. Kun, Mater. Sci. Forum 729 (2013) 68-73.
[39] X.F. Tao, L.P. Zhang, Y.Y. Zhao, Mater. Des. 30 (2009) 2732-2736.
[40] X. Xia, X. Chen, Z. Zhang, X. Chen, W. Zhao, B. Liao, B. Hur, Mater. Des. 56 (2014) 353-358.
[41] DIN50134 Testing of Metallic Materials—Compression test of metallic cellular materials, 2008.
[42] D.K. Balch, J.G. O'Dwyer, G.R. Davis, C.M. Cady, G.T. Gray III, D.C. Dunand, Mater. Sci. Eng. A 391 (2005) 408-417.
[43] D.K. Balch, D.C. Dunand, Acta Mater. 54 (2006) 1501-1511.
[44] Z.Y. Dou, L.T. Jiang, G.H. Wu, Q. Zhang, Z.Y. Xiu, G.Q. Chen, Scripta Mater. 57 (2007) 945-948.
[45] M.D. Goel, M. Peroni, G. Solomos, D.P. Mondal, V.A. Matsagar, A.K. Gupta, M. Larcher, S. Marburg, Mater. Des. 42 (2012) 418-423.
[46] M. Kiser, M.Y. He, F.W. Zok, Acta Mater. 47 (1999) 2685-2694.
[47] P.K. Rohatgi, A. Daoud, B.F. Schultz, T. Puri, Compos. Part A 40 (2009) 883-896.
[48] P.K. Rohatgi, N. Gupta, B.F. Schultz, D.D. Luong, JOM 63 (2011) 36-42.
[49] Z. Huang, S. Yu, J. Liu, X. Zhu, Mater. Des. 32 (2011) 4714-4719.
[50] Z.Q. Huang, S.R. Yu, M.Q. Li, Trans. Nonferrous. Met. Soc. China 20 (2010) 458-462.
[51] G. Castro, S.R. Nutt, Mater. Sci. Eng. A 535 (2012) 274-280.
[52] G. Castro, S.R. Nutt, X. Wenchen, Mater. Sci. Eng. A 578 (2013) 222-229.
[53] D.D. Luong, O.M. Strbik III, V.H. Hammond, N. Gupta, K. Cho, J. Alloys Compounds 550 (2013) 412-422.
[54] D.D. Luong, N. Gupta, A. Daoud, P.K. Rohatgi, JOM 63 (2011) 53-56.
[55] D.D. Luong, N. Gupta, P.K. Rohatgi, JOM 63 (2011) 48-52.

[56] B.P. Neville, A. Rabiei, Mater. Des. 29 (2008) 388-396.
[57] A. Rabiei, M. Garcia-Avila, Mater. Sci. Eng. A 564 (2013) 539-547.
[58] A. Rabiei, L.J. Vendra, Mater. Lett. 63 (2009) 533-536.
[59] L. Peroni, M. Scapin, M. Avalle, J. Weise, D. Lehmhus, Mater. Sci. Eng. A 552 (2012) 364-375.
[60] L. Peroni, M. Scapin, M. Avalle, J. Weise, D. Lehmhus, J. Baumeister, M. Busse, Adv. Eng. Mater. 14 (2012) 909-918.
[61] J.A. Santa Maria, B.F. Schultz, J.B. Ferguson, P.K. Rohatgi, Mater. Sci. Eng. A 582 (2013) 415-422.
[62] J.B. Ferguson, J.A. Santa Maria, B.F. Schultz, P.K. Rohatgi, Mater. Sci. Eng. A 582 (2013) 423-432.
[63] J.A. Santa Maria, B.F. Schultz, J.B. Ferguson, N. Gupta N, P.K. Rohatgi, J. Mater. Sci. 49 (2014) 1267-1278.
[64] X.F. Tao, Y.Y. Zhao, Scripta Mater. 61 (2009) 461-464.
[65] X.F. Tao, Y.Y. Zhao, Mater. Sci. Eng. A 549 (2012) 228-232.
[66] G.H. Wu, Z.Y. Dou, D.L. Sun, L.T. Jiang, B.S. Ding, B.F. He, Scripta Mater. 56 (2007) 221-224.
[67] L.C. Zou, Q. Zhang, B.J. Pang, G.H. Wu, L.T. Jiang, H. Su, Mater. Des. 45 (2013) 555-560.
[68] I.N. Orbulov, J. Ginsztler, Compos. Part A 43 (2012) 553-561.
[69] I.N. Orbulov, Mater. Sci. Eng. A 555 (2012) 52-56.
[70] I.N. Orbulov, Á. Németh, J. Dobránszky, J. Phys. Conf. Ser. 240 (2010) 1-4.
[71] I. N. Orbulov, Á. Németh, J. Ginsztler, Proceedings of International Conference on Cellular Materials. Dresden, Germany, 2010, pp. 377-82.
[72] L. Bardella, A. Sfreddo, C. Ventura, M. Porfiri, N. Gupta, Mechanics Mater. 50 (2012) 53-69.
[73] L. Bardella, F. Genna, Int. J. Sol. Struct. 38 (2001) 307-333.
[74] L. Bardella, Int. J. Eng. Sci. 41 (2003) 741-768.
[75] L. Bardella, F. Genna, Int. J. Sol. Struct. 38 (2001) 7235-7260.
[76] D.P. Mondal, N. Ramakrishnan, S. Das, Mater. Sci. Eng. A 433 (2006) 286-290.
[77] D.P. Mondal, N. Ramakrishnan, K.S. Suresh, S. Das, Scripta Mater. 57 (2007) 929-932.
[78] P.R. Marur, Mater. Lett. 59 (2005) 1954-1957.
[79] P.R. Marur, Acta Mater. 52 (2004) 1263-1270.
[80] P.R. Marur, Comp. Mater. Sci. 46 (2009) 327-332.
[81] P.R. Marur, Finite Elements in Analysis Des. 46 (2010) 1001-1007.
[82] I.N. Orbulov, K. Májlinger, Mater. Tehnol. 46 (2012) 375-382.
[83] I.N. Orbulov, K. Májlinger, Period. Polytech. Mech. Eng. 54 (2010) 89-94.
[84] I.N. Orbulov, J. Dobranszky, A. Nemeth, J. Mater. Sci. 44 (2009) 4013-4019.
[85] E. De Lorgeril, F. Wyss, I.N. Orbulov, Period. Polytech. Mech. Eng. 55 (2011) 29-37.
[86] I.N. Orbulov, K. Májlinger, Mater. Des. 49 (2013) 1-9.
[87] ASM Handbook. Properties and Selection: Nonferrous Alloys and Special-Purpose Materials, vol. 2. 2nd printing. ASM International, 1995, pp. 54.
[88] H.M. Jaeger, S.R. Nagel, Science 255 (1992) 1523-1531.
[89] S. Torquato, T.M. Truskett, P.G. Debenedetti, Phys. Rev. Lett. 84 (2000) 2064-2067.

**Table captions**

Table 1. The measured densities of the investigated MMSFs

| Reinforcement | Measured density, $\rho_m$ ($gcm^{-3}$) |
|---|---|
| 100GC (pure GC) | 1.833 |
| 80GC + 20GM | 1.743 |
| 60GC + 40GM | 1.694 |
| 40GC + 60GM | 1.649 |
| 20GC + 80GM | 1.639 |
| 100GM (pure GM) | 1.327 |

Table2. Strength properties and fracture strain of the investigated hybrid MMSFs

| Type | H/D | $\sigma_c$ (MPa) | $\sigma_y$ (MPa) | $\sigma_p$ (MPa) |
|---|---|---|---|---|
| 100GC (pure GC) | 1 | 114,5±4,01 | 113,0±4,01 | 88,1±8,40 |
| | 1.5 | 108,6±2,28 | 107,8±2,23 | 80,2±13,6 |
| | 2 | 106,0±4,26 | 108,7±4,51 | 75,5±16,6 |
| 80GC 20GM | 1 | 86,5±8,12 | 85,4±7,75 | 77,7±9,30 |
| | 1.5 | 82,4±7,03 | 82,0±6,99 | 70,0±9,82 |
| | 2 | 82,0±7,38 | 81,4±7,16 | 64,3±11,6 |
| 60GC 40GM | 1 | 77,5±11,1 | 74,6±11,1 | 71,2±13,4 |
| | 1.5 | 71,5±6,67 | 70,7±6,22 | 68,6±5,43 |
| | 2 | 68,6±9,30 | 64,7±11,9 | 62,3±11,2 |
| 40GC 60GM | 1 | 70,5±1,91 | 69,8±2,17 | 68,1±6,54 |
| | 1.5 | 64,6±4,77 | 61,1±4,00 | 66,2±12,9 |
| | 2 | 62,1±9,01 | 58,3±8,38 | 59,0±8,99 |
| 20GC 80GM | 1 | 65,9±5,05 | 59,7±7,36 | 64,5±7,14 |
| | 1.5 | 65,8±2,29 | 61,3±1,76 | 61,2±5,57 |
| | 2 | 60,0±3,81 | 60,0±3,81 | 57,1±8,45 |
| 100GM (pure GM) | 1 | 35,3±3,33 | 35,3±3,33 | 49,3±6,47 |
| | 1.5 | 37,6±1,57 | 37,6±1,57 | 48,1±9,18 |
| | 2 | 39,2±1,89 | 39,2±1,89 | 47,1±7,36 |

Table 3. Structural stiffness and absorbed energies of the investigated MMSFs

| Type | H/D | $\varepsilon_c$ (%) | S (MPa) | $W_c$ $Jcm^{-3}$ | W $Jcm^{-3}$ |
|---|---|---|---|---|---|
| 100GC (pure GC) | 1 | 3,20±0,274 | 4405±249,3 | 282,4±29,24 | 1959±20,3 |
| | 1.5 | 2,68±0,165 | 5914±355,4 | 199,1±21,16 | 1784±50,8 |
| | 2 | 2,25±0,063 | 7642±591,2 | 159,9±9,82 | 1611±51,9 |
| 80GC 20GM | 1 | 3,41±0,237 | 4283±358,9 | 199,6±27,70 | 1759±41,3 |
| | 1.5 | 2,63±0,140 | 5350±157,4 | 164,0±13,13 | 1666±49,5 |
| | 2 | 2,40±0,261 | 6160±291,8 | 153,0±27,99 | 1511±30,6 |
| 60GC 40GM | 1 | 3,63±0,505 | 3666±343,0 | 173,5±38,23 | 1515±55,2 |
| | 1.5 | 2,80±0,329 | 4924±140,2 | 133,1±29,86 | 1413±90,0 |
| | 2 | 2,72±0,612 | 4970±713,0 | 129,7±48,91 | 1378±63,0 |
| 40GC 60GM | 1 | 4,02±0,261 | 3582±135,6 | 208,5±17,50 | 1638±40,9 |
| | 1.5 | 3,72±0,381 | 4254±262,4 | 178,2±25,17 | 1504±67,9 |
| | 2 | 3,30±0,417 | 4483±846,5 | 179,2±19,69 | 1437±74,1 |
| 20GC 80GM | 1 | 6,03±0,644 | 2572±322,6 | 291,5±29,98 | 1571±67,2 |
| | 1.5 | 4,98±0,786 | 3654±266,3 | 252,8±50,69 | 1562±49,7 |
| | 2 | 4,46±1,345 | 4202±514,2 | 213,7±80,82 | 1473±77,1 |
| 100GM (pure GM) | 1 | - | 2369±51,9 | - | 1128±67,0 |
| | 1.5 | - | 3222±14,4 | - | 1212±63,8 |
| | 2 | - | 3994±108,2 | - | 1238±33,0 |

**Figure captions**

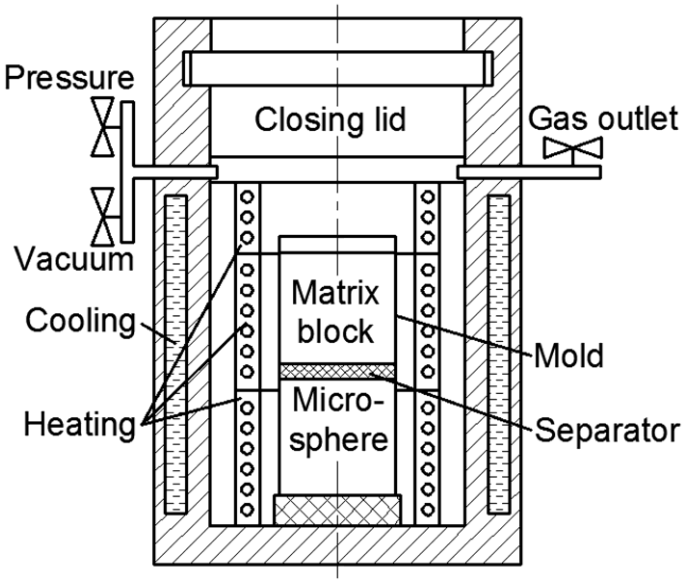


Fig. 1. Schematic sketch of the infiltration chamber

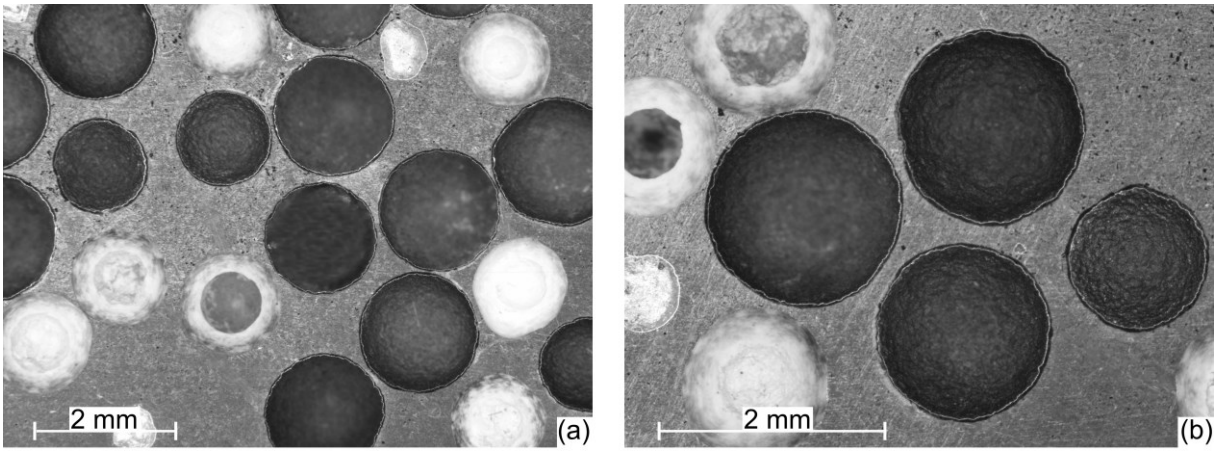


Fig. 2. Micrographs about typical areas of 20GC+80GM ASFs

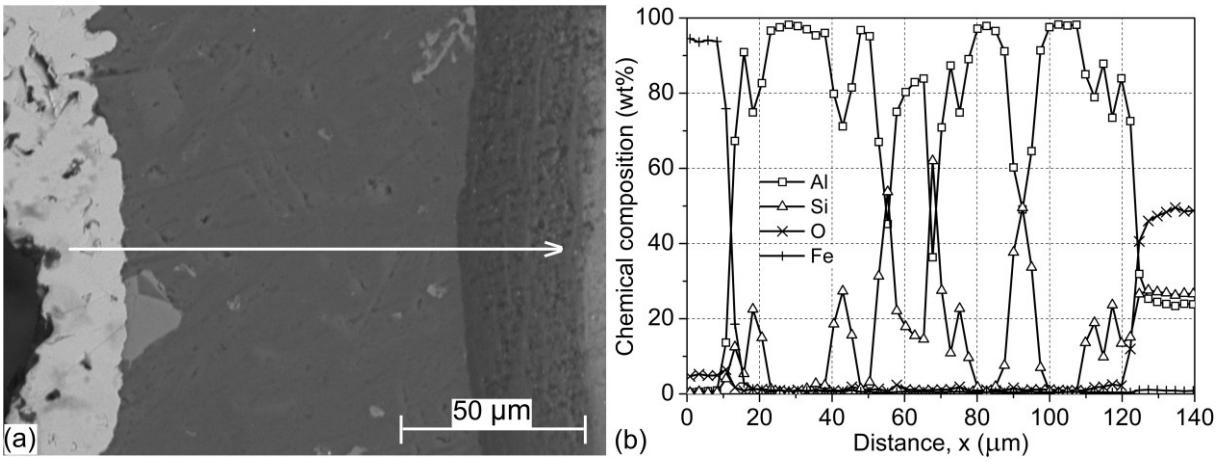


Fig. 3. BSE image (a) of a GM (left) and a GC (right) grade hollow sphere and EDS line-scan profile (b) of 60GC+40GM ASF

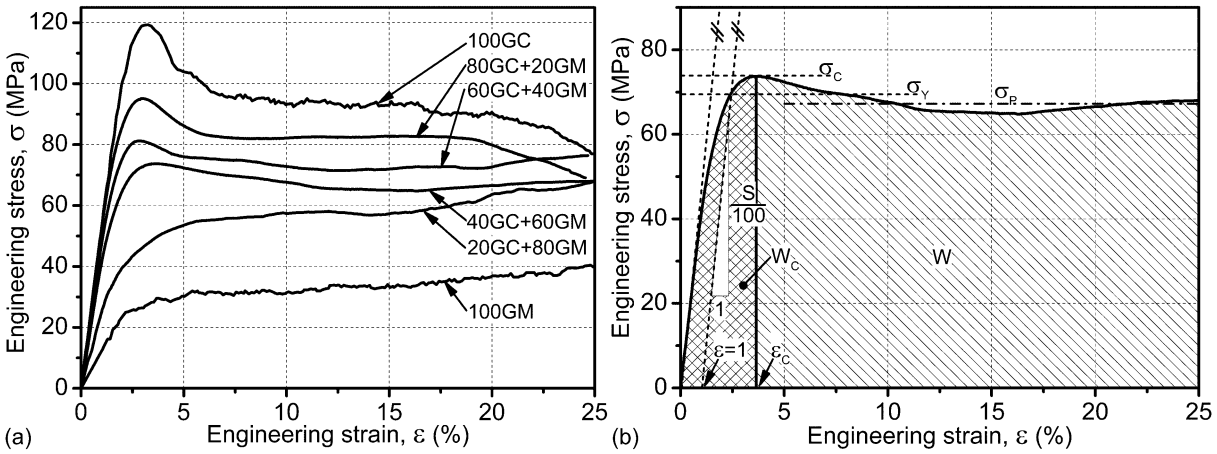


Fig. 4. Typical engineering stress – engineering strain curves of ASFs (H/D=1) (a) and the monitored properties (b)

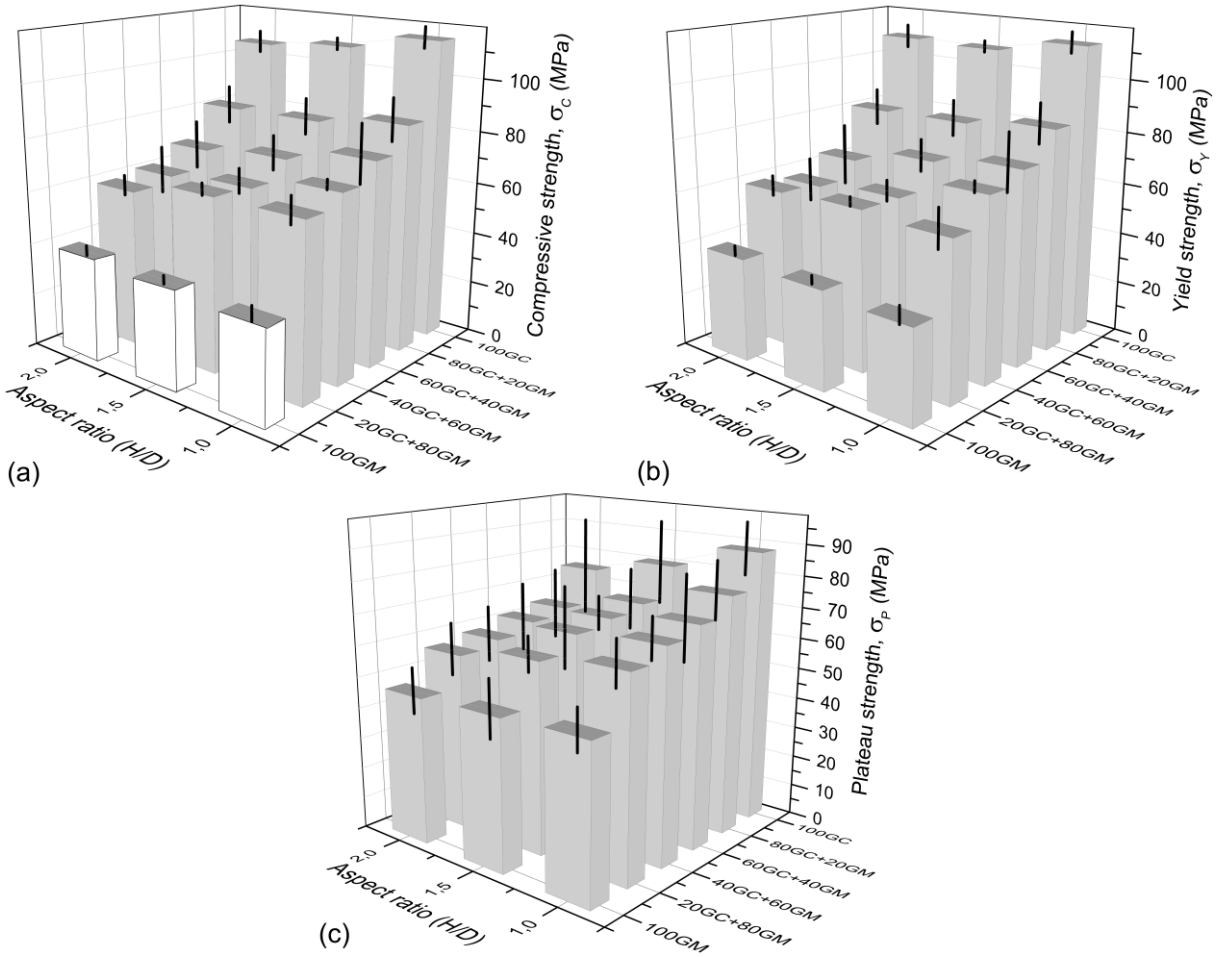


Fig. 5. The average compressive (a) yield (b) and plateau (c) stress of ASFs in the function of hollow sphere grade and aspect ratio

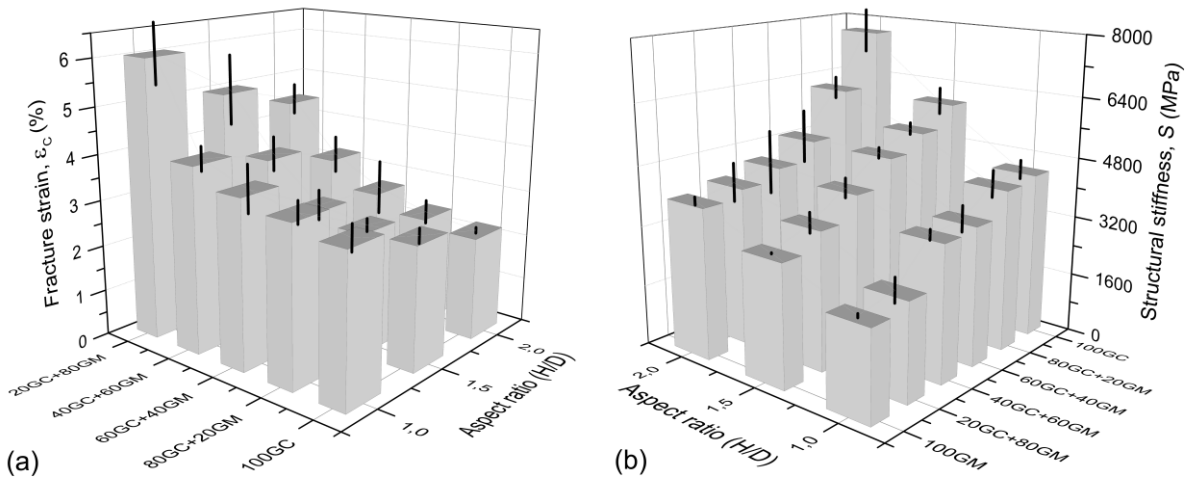


Fig. 6. The fracture strain (a) and the structural stiffness (b) of ASFs as the function of hollow sphere grade and aspect ratio

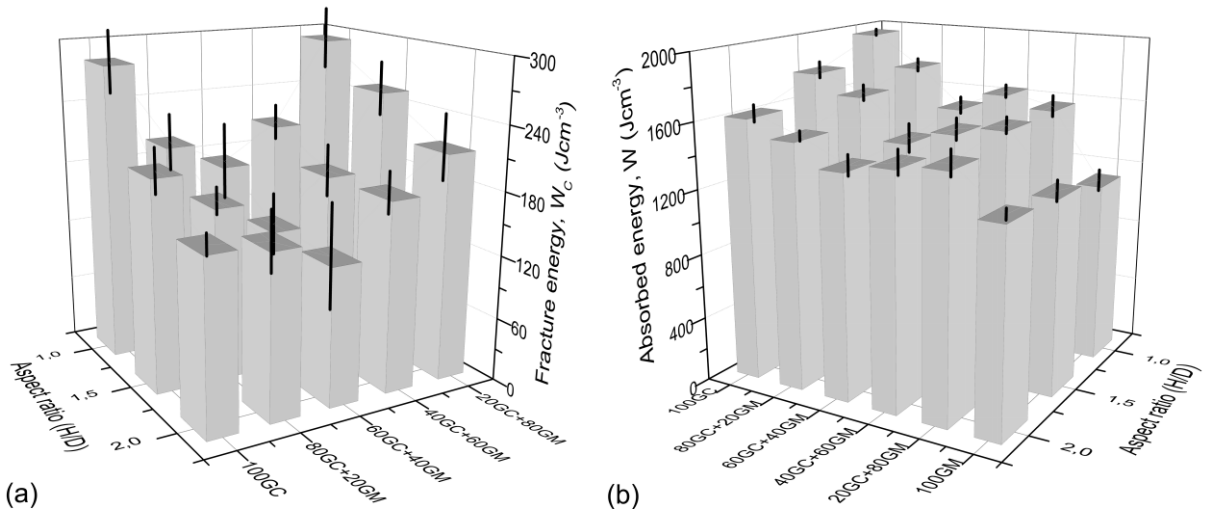


Fig. 7. The fracture energy (a) and the absorbed energy (b) of ASFs as the function of hollow sphere grade and aspect ratio

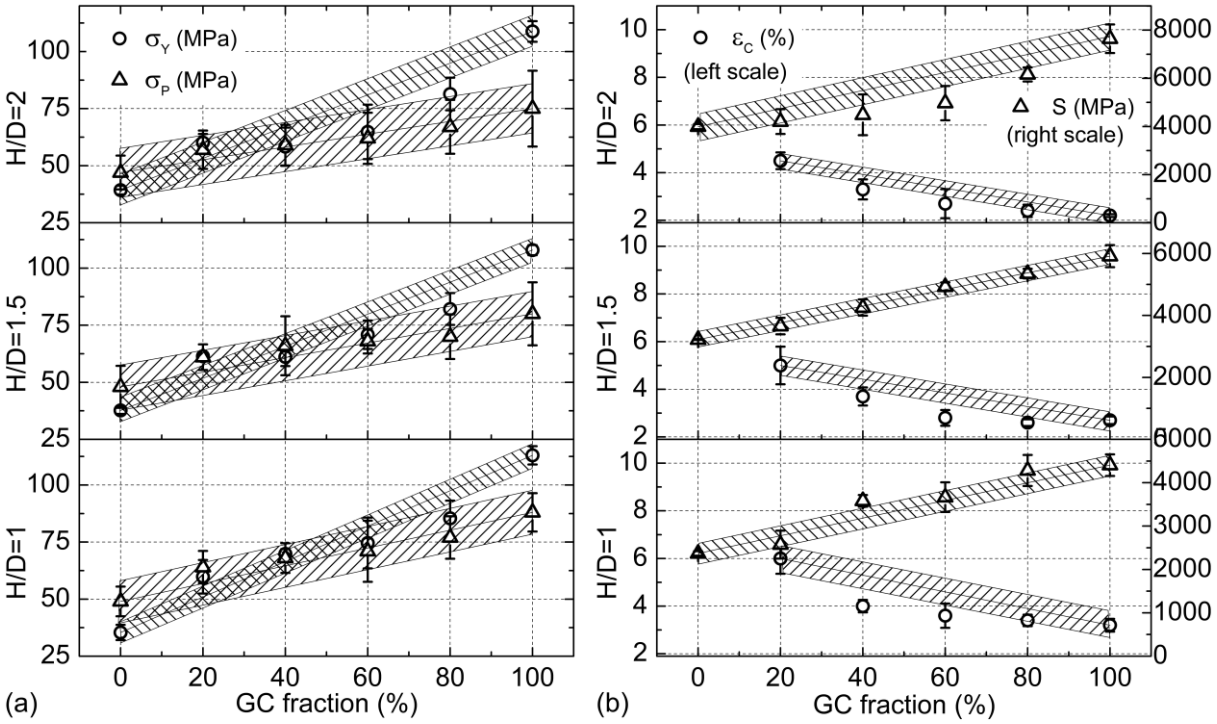


Fig. 8. Representation of the rule of mixtures in the case of (a) yield and plateau strength and (b) structural stiffness and fracture strain

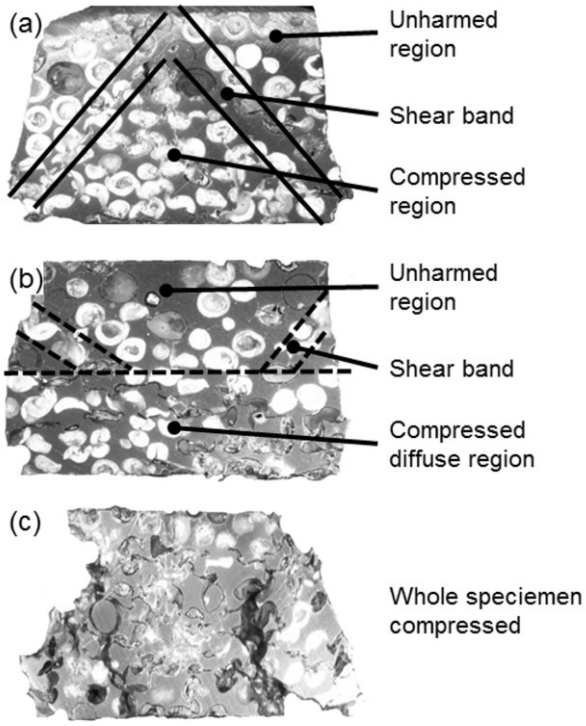


Fig. 9. Macrographs about the failure mechanisms of AFs (a) brittle fracture (80GC+20GM), (b) transient failure mode (40GC+60GM) and (c) diffuse plastic deformation (20GC+80GM)